Mugla Journal of Science and Technology

A COMPUTATIONALLY EFFICIENT ENERGY MANAGEMENT STRATEGY FOR A PLUG-IN FUEL-CELL HYBRID ELECTRIC VEHICLE COMPOSED OF A MULTI-INPUT CONVERTER

*Furkan AKAR
Electrical and Electronics Engineering Department, Technology Faculty, Duzce University, Turkey, furkanakar@duzce.edu.tr-
https://orcid.org/0000-0002-1460-4468

Received: 15.10.2018, Accepted: 08.03.2019 Research Article
*Corresponding author DOI: 10.22531/muglajsci. 482934

Abstract

Fuel cell vehicle technology has drawn wide attention because of the environmental and economic issues related to excessive usage of fossil fuels. Fuel cells are known for their unidirectional environmental friendly operation; however, they have low power density and suffer from slow dynamics. Therefore, a sole fuel cell system cannot meet the requirements of an electric vehicle whose power demand is quite dynamic. In a way of hybridizing a fuel cell with energy storage devices, it can be possible to overcome aforementioned problems. A plug-in fuel cell hybrid electric vehicle system, equipped with a battery and an ultra-capacitor, is proposed in this work. In this system, a single multi-input converter is utilized to control source energies. Moreover, this work develops a computationally efficient energy management strategy which is essentially a frequency decoupling method basically taking the advantage of easily applicable low pass filters. In this strategy, a polynomial scales the fuel cell and battery power levels to regulate ultra-capacitor voltage. The whole system is tested via a simulation model after the detailed analysis of the multi-input converter.

Keywords: Fuel cell, battery, ultra-capacitor, electric vehicles, multi-input converter, energy management.

ÇOK GİRİŞLİ DÖNÜŞTÜRÜCÜDEN OLUŞAN ŞARJ EDİLEBİLİR YAKIT HÜCRELİ BİR HİBRİT ELEKTRİKLİ ARAÇ İÇİN HESAPLAYICI VERİMLİ BİR ENERJİ YÖNETİM YÖNTEMİ

Özet

Fosil yakıtların aşırı kullanımının oluşturduğu çevresel ve ekonomik kaygılardan dolayı, yakıt hücreli araç teknolojisi oldukça ilgi çekmektedir. Yakıt hücresi sistemleri tek yönlü çevre dostu işletimleriyle bilinmektedir, ancak güç yoğunlukları düşük ve tepki süreleri yavaştır. Dolayısıyla, bir yakıt hücresi sistemi, güç talebi oldukça dinamik olan bir elektrikli aracın ihtiyacına tek başına cevap verememektedir Yakıt hücresi sistemlerini enerji depolama sistemleri ile birlikte kullanarak bahsedilen problemlerin üstesinden gelinebilir. Bu çalışmada batarya ve ultra-kapasitör içeren şarj edilebilir yakıt hücreli bir hibrit elektrikli araç sistemi sunulmaktadır. Bu sistemde, bir adet çok-girişli dönüştürücü kullanılarak kaynak enerjileri kontrol edilmektedir. Ayrıca, bu çalışma hesaplayıcı verimli bir enerji yönetim stratejisi geliştirmektedir. Temelde bu strateji kolay uygulanabilen alçak geçiren filtrelerden yararlanan bir frekans ayırma yöntemidir. Bu stratejide, bir polinom yakıt hücresi ve batarya güçlerini ölçeklendirerek ultra-kapasitör gerilimini regüle etmektedir. Tüm sistemin çalışması, çok girişli dönüştürücün detaylı analizinden sonra, bir benzetim çalışması ile test edilmektedir.

Anahtar Kelimeler: Yakıt hücresi, batarya, ultra-kapasitör, elektrikli araçlar, çok-girişli dönüştürücü, enerji yönetimi.

Cite

Akar, F., (2019). "A computationally efficient energy management strategy for a plug-in fuel-cell hybrid electric vehicle composed of a multi-input converter", Mugla Journal of Science and Technology, 5(1), 52-60.

1. Introduction

Plug-in fuel-cell hybrid electric vehicles (PFCHEVs) come to forefront among EVs; since they offer many advantages; such as, long travel distance, fast charge, high energy/power density, etc [1]-[3]. A PFCHEV includes a hybrid power system (HPS) gathering a fuel-cell (FC) with an energy storage system (ESS) to promote FC lifetime, to increase power density and to allow fuel economy [3]. Source energies in HPSs are controlled via power electronics structures according to an energy management strategy (EMS). One of the methods offered in the literature for HPSs is to connect some sources directly to the dc bus while controlling other source energies by bidirectional or unidirectional dc-dc converters [4, 5]. Even though these kinds of semi-active structures are simple and efficient, they do not allow to adjust dc bus voltage and source power levels effectively In addition, works in [6, 7] propose separate converters for each source in order to overcome the issues associated with the semi-active structures at the expense of increased cost and complexity. The other method benefits

from the multi-input converters (MICs), which have several advantages over multiple converter approach; e.g. compact design, low component count, and high energy density [8, 9].

There are two popular structures in the literature for a PFCHEV: FC/ultra-capacitor (UC) and FC/battery/UC. In [6], it is showed that FC/battery/UC system is preferable to FC/UC system when considering many parameters; such as, system size, fuel economy, and battery life time. The proposed FC/battery/UC system in [10] is basically a semi-active topology in which two separate dc-dc converters are used for FC and battery while UC is directly linked to the dc bus. Moreover, [11] offers a similar semi-active system for a FC electric bus in a way of connecting battery to the dc bus directly and utilizing two different dc-dc converters for FC and UC. Furthermore, authors create an active FC/battery/UC hybrid EV in [12] through three separate converters. The studies in [13] and [14] propose FC/battery/UC drive-trains based on a power electronic structure called multiple-input power electronic converter which essentially consists of three bi-directional step-up/step-down dc-dc converter connected in parallel. Moreover, [15] proposes a three-input dc-dc converter which can effectively build an active FC/battery/UC hybrid system; however, it has only boost capability when powering the output. Additionally, the converter in [15] does not have a common ground that can result in electromagnetic inference (EMI) noise. Unlike the previous studies explored above, an active FC/battery/UC hybrid system is created in this work based on a single MIC which has a common ground as well as buck and boost capabilities. Moreover, this paper offers a new computationally efficient EMS whose details can be found in Section 3.

The MIC used in this work is shown in Fig. 1(a). This MIC is evaluated in [16] when it has 2 inputs. Moreover, 3-input case is studied in [17] via an ideal switching model. Although demonstrated simulation results in [17] are quite satisfying for judging the operational capability of the MIC, the given analysis ignores non-idealities and does not evaluate the dynamic performance of the MIC. Contributions of this work can be summarized as follows:

1) A non-ideal non-linear average model of the studied MIC for 3-input case is given for the first time; therefore, the analysis is novel and simulation study is quite realistic.
2) A new low complexity energy management strategy based on frequency decoupling for a PFCHEV is proposed.
3) A control strategy is developed to maximize the efficiency.

2. Analysis of MIC

As shown in Fig. 1(b), there are two main operation modes: motoring mode and regenerative mode. In motoring mode, the inverter powers the motor when EV is accelerating; moreover, FC and battery always discharge. When it comes to UC, two cases happen: UC also discharges in Case-1, and UC is charged by FC and battery in Case-2. Additionally, in regenerative mode, the inverter transfers the regenerative braking energy from the motor when EV is decelerating; UC stores this energy as shown in Fig.1 (b). Here, the battery is not charged though it is possible since it is addressed in [12] that frequent charges can shorten the battery lifetime.

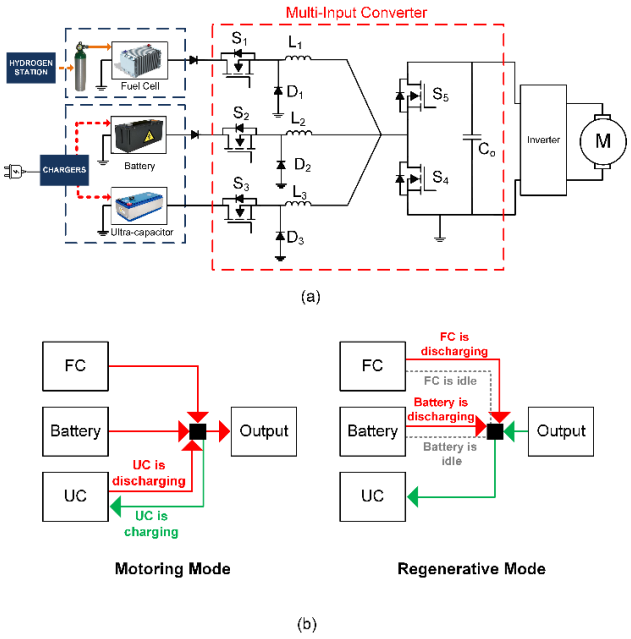

Figure 1. a) Structure for proposed plug-in fuel cell hybrid electric vehicle, b) its operation modes.

There are also two cases in regenerative mode: FC and battery discharge so as to increase UC charging current in Case-1, and they become idle in Case-2. Note that Case-1 in regenerative mode is activated when UC state-of-charge (SOC) is low.

The analysis is realized for Continuous Conduction Mode (CCM) and it is assumed that the output capacitor is ideal and large enough to maintain a constant output voltage during one switching period. Besides, in order to make the analysis realistic, parasitic elements are taken into account, these elements are on-time resistance of switches ($R_{ds\text{-}on}$), the voltage drop on body diodes of switches (V_{SD}), inductor equivalent series resistance (R_L), and the forward voltage drop on diodes (V_F). Duty cycles of S_1, S_2, S_3, S_4, and S_5 are d_1, d_2, d_3, d_4, and d_5, respectively, while T_s is the switching period. Here it is assumed that $v_{FC} > v_o > v_{bat} > v_{UC}$ where v_{FC}, v_o, v_{bat}, and v_{UC} are the instantaneous voltages of FC, output, battery and UC, respectively.

2.1. Motoring Mode

Typical waveforms for this mode are given in Fig. 2(a) while associated equivalent circuits in two cases can be found in Fig. 3 and Fig. 4. In this mode, S_1, S_2, and S_4 are controlled by pulse-width-modulation (PWM) while S_5 is always OFF. The output current, i_o, is always positive in this mode.

2.1.1. Case 1

In Case-1, all sources discharge therefore all inductor currents are positive. As illustrated by the typical waveforms in Fig.3, there are 5 distinct subintervals in one switching period for this case. By examining these subintervals, the non-ideal inductor voltages can be written in Appendix-A as given in (A.1)-(A.3).

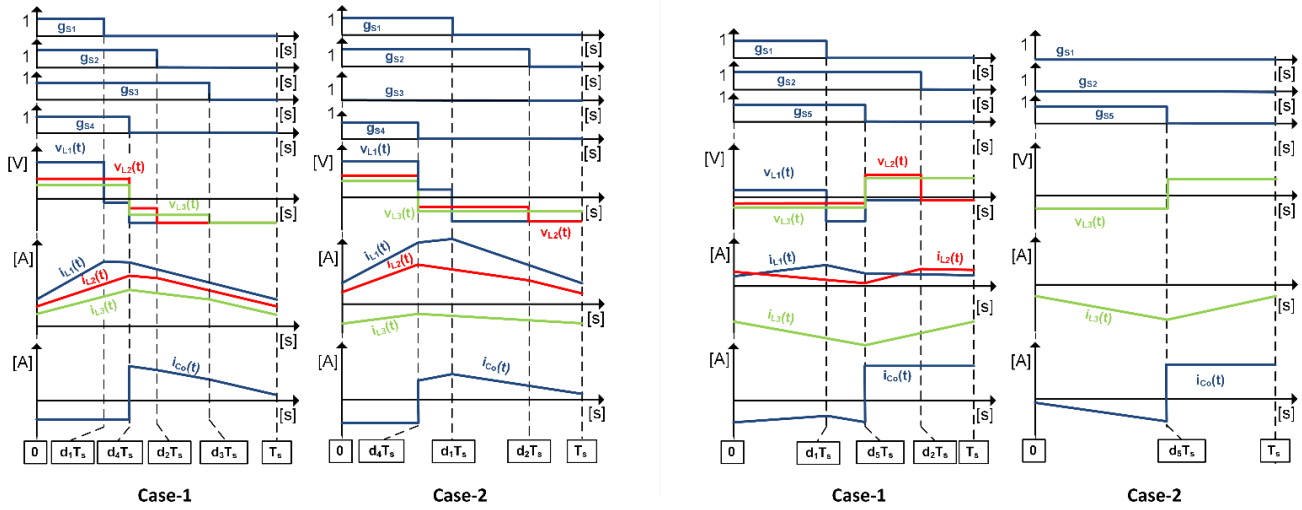

(a) (b)

Figure 2. Typical waveforms for a) motoring mode, b) regenerative mode.

In (A.1)-(A.3), $\sum i_L$ is the total inductor current which is basically equal to $i_{L1}+i_{L2}+i_{L3}$. After applying small-ripple-approximation (SRA) and volt-second-balance (VSB) principles to these equations, the non-ideal voltage equation in this case can be calculated as in (1).

$$V_0 = \Big[V_i D_i - I_{L-i}(R_{DS-ON}D_i + R_L) - \Big(\sum I_L\Big)(R_{DS-ON}D_4) - V_F(1-D_i) - V_{SD}(1-D_4)\Big]\Big[\frac{1}{(1-D_4)}\Big] \quad (1)$$

In (1), i index takes values of 1, 2, and 3 since the MIC has 3 inputs. Here, the voltages are steady state voltages which are $V_1 = V_{FC}$, $V_2 = V_{bat}$, and $V_3 = V_{UC}$. Other terms are also associated steady state quantities. For the ideal case, (1) becomes $V_0 = V_i D_i/(1-D_4)$. Thus, D_4 can be set to any value here that makes power transfer possible according to voltage levels. The output capacitor current is equal to the negative output current, $-i_o$, in first two subintervals, while it is equal to $\sum i_L - i_o$ in other subintervals. By SRA and VSB, the current equation at steady state can be computed as in (2).

$$I_0 = \Big(\sum I_L\Big)(1-D_4) \quad (2)$$

2.1.2. Case 2

In Case-2, UC is charged by FC and battery. This case happens when SOC of UC is low. Here S_3 is not controlled anymore since its body diode starts to conduct to carry negative L_3 current. Fig. 2(a) shows the typical waveforms for this case consisting of four distinct subintervals in one switching period. Furthermore, equivalent circuits are given in Fig. 4.

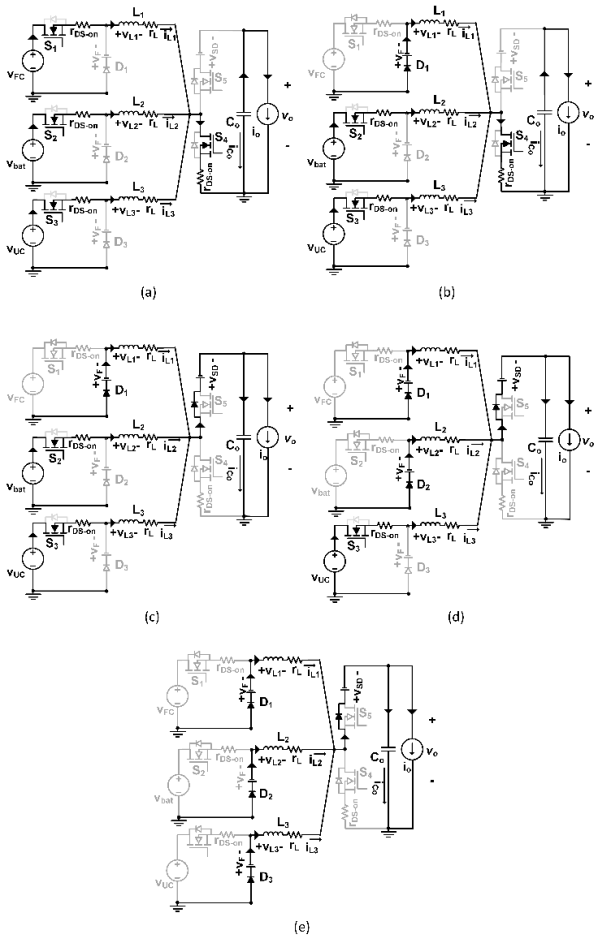

Figure 3. Equivalent circuits for motoring mode in Case1

for a)$0\sim d_1T_S$, b)$d_1T_S\sim d_4T_S$, c)$d_4T_S\sim d_2T_S$, d)$d_2T_S\sim d_3T_S$, e)$d_3T_S\sim T_S$.

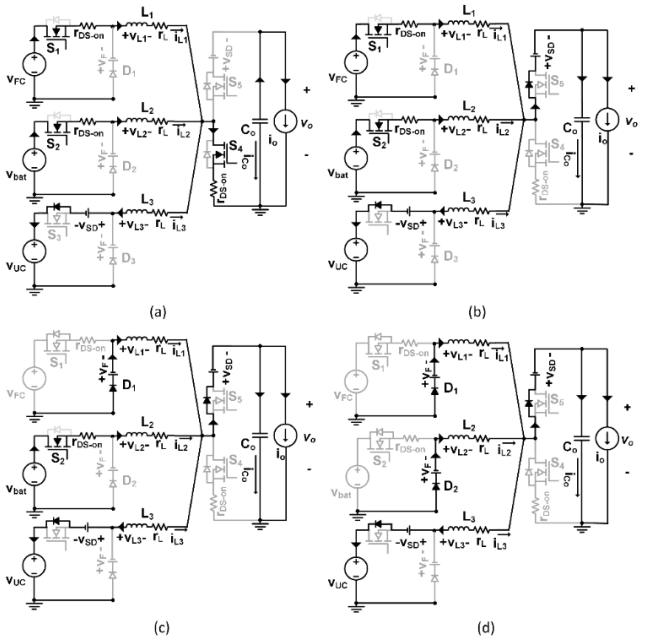

Figure 4. Equivalent circuits for motoring mode in Case2 for a) $0\sim d_4T_S$, b)$d_4T_S\sim d_1T_S$, c)$d_1T_S\sim d_2T_S$, d) $d_2T_S\sim T_S$.

As can be seen by comparing Fig. 4 and Fig. 5, equivalent circuits for Case-1 and Case-2 are same for FC and battery inputs. L_3 voltage variations in this case for UC input can be given as in (A.4). Furthermore, the non-ideal voltage equation in this case for UC input can be given as in (3).

$$V_0 = \left[V_{UC} - I_{L3}R_L - \left(\sum I_L\right)(R_{DS-ON}D_4) - V_{SD}D_4\right]\left[\frac{1}{(1-D_4)}\right] \quad (3)$$

For the ideal case, the steady state voltage relationship in Case-2 becomes $V_0 = V_{FC}D_1/(1-D_4) = V_{bat}D_2/(1-D_4) = V_{UC}/(1-D_4)$ Therefore, unlike the Case-1, D_4 needs to be controlled in this case to charge UC while D_1 and D_2 are controlled for adjusting L_1 and L_2 currents. The current equation in Case-2 can be found as in (2).

2.2. Regenerative Mode

Typical waveforms and equivalent circuits for regenerative mode are given in Fig. 2(b), Fig. 5 and Fig. 6, respectively. In the regenerative mode, S_1, S_2, and S_5 are controlled by PWM while S_3 and S_4 are always OFF. Because of the regenerative braking energy, the output current becomes negative.

2.2.1. Case 1

In Case-1, UC is charged by the regenerative braking energy and energies coming from FC and battery. Thus, L_1 and L_2 currents are positive while L_3 current is negative. According to Fig. 2(b) and Fig. 5, Case-1 includes 4 different subintervals in one switching period. According to these subintervals, the non-ideal inductor voltages in Case-1 for regenerative mode can be collected as in (A.5)-(A.7). Then, the non-ideal voltage equation for FC and battery inputs in this case can be calculated as follows:

$$V_0 = \left[V_i d_i - I_{L-i}(R_{DS-ON}D_i + R_L) - \left(\sum I_L\right)(R_{DS-ON}D_5) - V_F(1-D_i) + V_{SD}(1-D_5)\right]\left[\frac{1}{D_5}\right] \quad (4)$$

In (4),i index takes values of 1 and 2. Additionally, the non-ideal voltage equation for UC input is given in (5).

$$V_0 = \left[V_{UC} - I_{L3}R_L - \left(\sum I_L\right)(R_{DS-ON}D_5) - V_{SD}(2-D_5)\right]\left[\frac{1}{D_5}\right] \quad (5)$$

For the ideal case, the steady state voltage relationship in Case-1 is $V_0 = V_{FC}D_1/D_5 = V_{bat}D_2/D_5 = V_{UC}/D_5$ Therefore, D_5 is controlled here to store regenerative braking energy in UC while D_1 and D_2 are again controlled for adjusting L_1 and L_2 currents. This relationship also suggests that charging an input from the output or another input can be realized by only bucking capability.

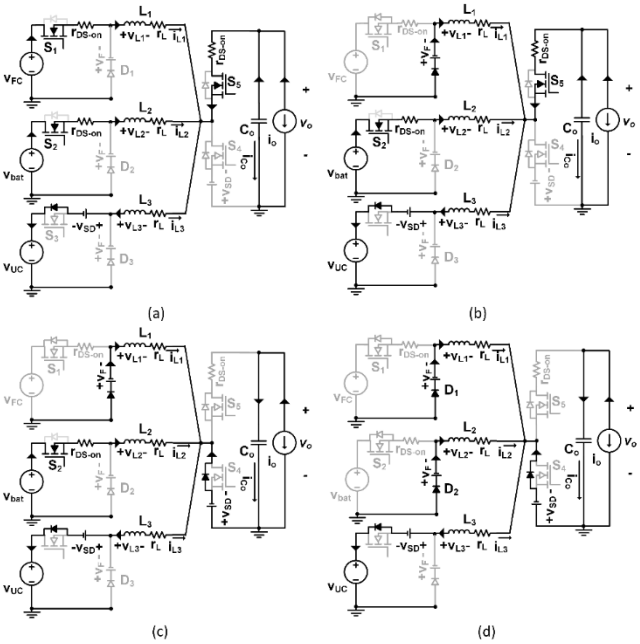

Figure 5. Equivalent circuits for regenerative mode in Case1 for a)$0\sim d_1T_S$, b)$d_1T_S\sim d_5T_S$, c) $d_5T_S\sim d_2T_S$, d) $d_5T_S\sim T_S$.

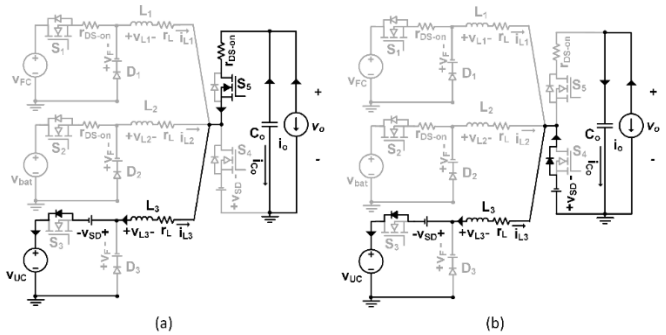

Figure 6. Equivalent circuits for regenerative mode in Case2 for a)$0\sim d_5T_S$, b)$d_5T_S\sim T_S$.

The output capacitor current is equal $\sum i_L - i_o$ in the first two intervals while it is equal to $-i_o$ in other subintervals. By SRA and VSB, current equation at steady state can be computed as in (6).

$$I_0 = \left(\sum I_L\right) D_5 \tag{6}$$

2.2.2. Case 2

In this case, UC is charged by only the regenerative braking energy. Therefore, L_1 and L_2 currents are zero whereas L_3 current is negative. S_5 is controlled by PWM and there are two subintervals in one switching period as shown in Fig. 2(b) and Fig. 6. The non-ideal voltage equation and current equation for UC input in this case are identical to (5) and (6), respectively.

3. Energy Management and Control Strategies

So as to split power demand in hybrid EVs, researchers have proposed many EMSs which can be divided into four main categories according to [18]. The first category consists of intelligent-based EMSs using methods like fuzzy-logic (FL) [19] and neural network [20]. In the second category, there are optimization based EMSs utilizing methods like particle-swarm-optimization [21] and genetic algorithm [22]. The third category includes frequency decoupling based EMSs that basically aim to prevent FC from load changes with high frequencies; in this category, filters [23] and wavelet transformation (WT) [24] are used. The last category contains EMSs based on various methods, such as, adaptive control [25], flatness control [26], etc. Among these strategies, filter based frequency decoupling EMS have drawn wide attention thanks to their effectiveness and simple structures [27]. For instance, in [23], authors propose an EMS, based on a first-order low pass filter, which successfully smooths FC power profile; however, it does not offer a way to realize voltage regulation and power management for the ESS. Moreover; in [28], a high-pass filter is used to separate output current into high and low frequency components for a battery/UC EV. In addition to achieved good power decoupling performance, the method in [28] effectively keeps both source voltages in determined limits through low-order transfer functions, saturations, multiplications, and divisions. EMSs similar to [28] can be found in [29-32]. Unfortunately, EMSs in [28-32] are not applicable to FC/battery/UC hybrid systems; in order to develop frequency decoupling based EMSs feasible to these systems, researchers have mostly focused on WT [24], [33]. WT mainly decomposes a signal into components at different positions and scales by utilizing two different transfer functions for decomposition and reconstruction steps. As an alternative to WT-based EMSs, this paper proposes an EMS which mainly consists of only two low pass filters (LPFs) and a polynomial function. The proposed EMS can be seen in Fig. 7. In the proposed EMS, first of all, the output power is filtered by a Low Pass Filter (LPF) whose time constant is 10s. Then, the output of this LPF is injected to another LPF whose time constant is 20s. Time constants of the filters are determined based on several preliminary simulation studies. The second LPF output is scaled by a cubic polynomial whose output is represented by α. From Fig. 7, it can be seen that this scaling factor becomes 1 when SOC_{UC} is 0.5, 2 when SOC_{UC} is 0, and 0 when SOC_{UC} is 1. Therefore, it is aimed to adjust the total power reference of FC and battery so as to keep SOC_{UC} around 0.5. Coefficients of this polynomial from the leading one to the constant one are found as -7.19, 10.79, -5.56, and 1.98, respectively. After a saturation block, FC reference power ($P_{FC\text{-}ref}$) is determined. Furthermore, the difference between the first LPF output and $P_{FC\text{-}ref}$ is also scaled by α and subjected to a saturation block; by this way, battery reference power is calculated. Through the proposed EMS, FC and battery attend the low frequency part of power demand while UC handles the transient power variations and regenerative braking energy capturing. According to determined reference power levels of FC and battery, d_1 and d_2 are controlled via two proportional-integral (PI) controllers. For Case-1 in motoring mode, d_4 is calculated by (7).

$$d_{4-opt} = 1 - \frac{min(v_{FC}, v_{bat}, v_{UC})}{v_{out}}\beta \tag{7}$$

In [16], it is shown that efficiency increases when d_4 is decreased; therefore (7) basically sets d_4 to the lowest possible value according to voltage levels of inputs and output which are associated with (1). In (7), β is adjustment coefficient for taking into account the non-idealities. In Case-1, d_3 is adjusted by a PI controller for regulating the dc bus; hence UC power is controlled. For Case-2 in motoring mode, d_3 is set to zero while d_4 is controlled for dc bus regulation in a way of charging UC accordingly. In regenerative mode, both d_3 and d_4 are zero since output and UC currents are now negative. Here, d_5 is adjusted by a PI controller for dc bus regulation.

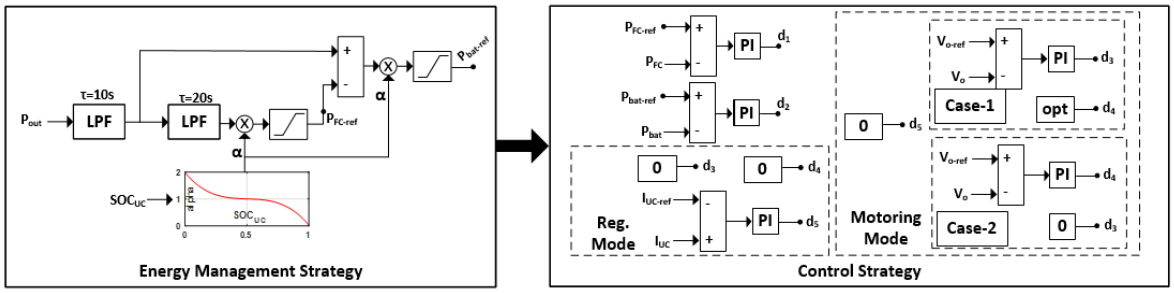

Figure 7. Proposed EMS and control strategy.

4. Simulation Study

According to [10], the component sizing in a PFCHEV is crucial to maximize the fuel economy, reliability, and performance while minimizing cost. Since this paper focuses on an EMS for a PFCHEV composed of a MIC, optimal sizing values given in [10] are utilized. Therefore, the maximum power levels are determined as 40-kW, 52-kW, 120-kW, for FC, battery bank (270-V, 450-Ah), and UC bank (432-V, 10.7-F), respectively; whereas, the maximum output power of 160-kW. Then, the simulation models of FC, battery, and UC are built as in [10]. Based on the determined power levels and structure of the studied MIC, the maximum voltages and currents are selected as 400-V and 130-A for FC input; 315-V and 190-A for battery input, 432-V and 600-A for UC input. Moreover, the output voltage reference is set to 300-V, while the maximum output current is calculated as 533-A. Finally, the converter is designed by following the procedure given in [12]. The selected metal-oxide-semiconductor field-effect transistor (MOSFET) is IXFK80N60P3 (600-V, 80-A), while the diode is RURF8060 (600-V, 80-A). V_{SD} and R_{DS-ON} for this MOSFET is 1.5-V and 70-mΩ, respectively, while V_F for the diode is about 1.6-V. Note that, MOSFETs and diodes are paralleled to increase current handling capability. The number of parallel MOSFETs and diodes are 5, 9, 22, and 20 for FC, battery, UC, and output ports, respectively. Furthermore, for 20-kHz switching frequency and 20% current ripple, calculated inductor values are 150-µH, 80-µH, and 40-µH; while R_L values are 30-mΩ, 22-mΩ, and 15-mΩ for L_1, L_2, L_3, respectively [12]. According to given parameters, a non-ideal non-linear model [12] of the MIC is created in MATLAB/SIMULINK based on (1)-(6) as illustrated in Fig. 8.

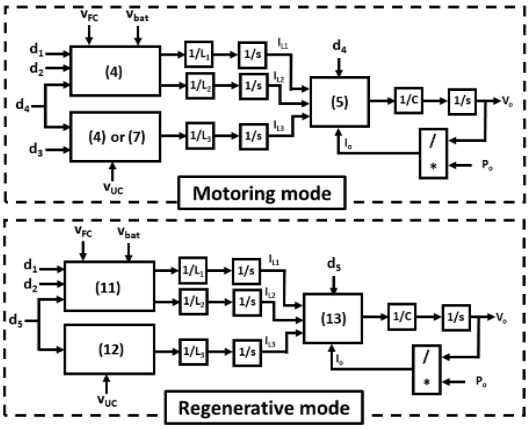

Figure 8. Schematic of the simulation model of MIC.

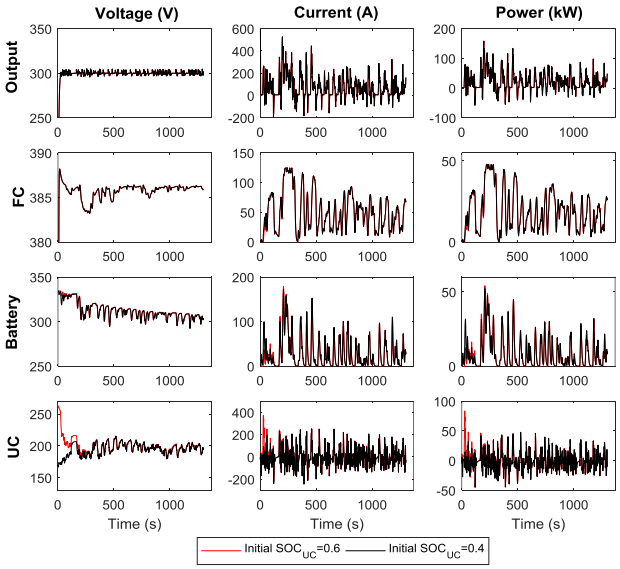

Figure 9. Simulation results: terminal voltages, currents and powers.

4.1. Simulation Results

Fig.9 shows voltage, current and power variations of the output and input sources for two different values of initial SOC_{UC}, 0.4 and 0.6. Here, the output power profile is obtained according to ECE-15 standardized urban driving cycle [34]. First of all, it can be noticed that the output voltage is successfully kept around 300-V in both cases.

This observation clearly reveals that the MIC realizes the power flow properly. Additionally, one can see from FC power variations in Fig.9 that FC does not experience transient changes in both cases. In other words, FC supplies the base load. Therefore, FC lifetime can be increased through the hybridization in comparison to a solely FC system [12]. Moreover, maximum FC power levels are about 40-kW in accordance with the design parameter. According to Fig.9, the battery supports FC in supplying steady the state load demand; therefore it is

not affected by sudden load changes. Furthermore, the battery never captures the regenerative braking energy. This strategy obviously results in a degradation in its voltage; however, it can help to extend the battery lifetime by avoiding frequent charges [12]. Moreover, the peak battery powers in both cases are about 50-kW as aimed.

Since initial values of SOC_{UC} are set to 0.4 and 0.6, UC voltages are approximately 170-V and 260-V at the beginning of the simulation. The proposed EMS aims to regulate SOC_{UC} around 0.5; therefore, UC voltage should be around 216-V. From Fig.10, it can be clearly seen that UC voltage first increases for SOC_{UC}=0.4 while it first decreases for SOC_{UC}=0.4; then, the EMS pushes UC voltages to oscillate around 216-V in both cases. According to this investigation, one can clearly comment that the scaling factor is determined properly, and the offered method based on this procedure accomplishes SOC_{UC} regulation.

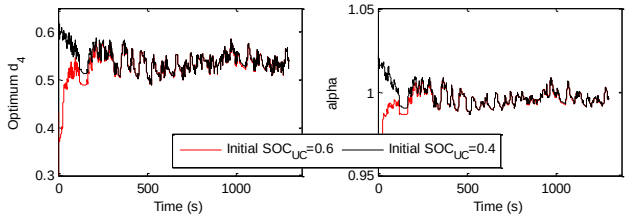

Figure 10. Simulation results: Optimum d_4 and α in EMS.

Finally, Fig. 10 demonstrates the optimum d_4 values and the scaling factors (α). At the beginning of the simulation, the optimum d_4 values are about 0.6 and 0.4 for the initial SOC_{UC} values of 0.4 and 0.6, respectively. Then they start to oscillate smoothly around 0.55 thanks to regulated SOC_{UC}. Similar to d_4, α first decreases for the initial SOC_{UC}=0.4, and increases for the initial SOC_{UC}=0.6. Finally, it takes values around 1 as an indication of regulated SOC_{UC}.

In order to evaluate the frequency decoupling performance of the proposed EMS, absolute values of rate of power changes are calculated for two simulation cases; then, they are averaged over the simulation time. As given in Table 1, these values are denoted by $\overline{|\Delta P_{out}/\Delta t|}$, $\overline{|\Delta P_{FC}/\Delta t|}$, $\overline{|\Delta P_{bat}/\Delta t|}$, and $\overline{|\Delta P_{UC}/\Delta t|}$ for the output, FC, battery and UC, respectively. As can be seen from this table, similar results are obtained in two cases. Additionally, FC has the smoothest power profile as can be understood from that $\overline{|\Delta P_{FC}/\Delta t|}$ takes the lowest values. In addition, battery experiences slightly more rate of power change when compared to FC. Actually, this is an expected result due to the different time constants utilized in LPFs. Moreover, the results for $\overline{|\Delta P_{UC}/\Delta t|}$ obviously verify that the UC undertakes the transient power changes.

5. Conclusion

This work has proposed a PFCHEV system utilizing a single MIC. A non-ideal non-linear average model of the MIC has been constructed according to a detailed analysis and a design procedure. Then, a computationally efficient EMS, which aims to allocate the load demand according to the characteristics of sources, has been proposed. According to simulation results, the average output voltage errors are computed as about 1% under ECE-15 driving cycle. Moreover, UC has experienced almost 5 times greater rate of power change than FC and battery. Therefore, it is clear that the offered system along with the EMS effectively hybridize FC, battery and UC; and it is promising in terms of enhancing the lifetimes of FC and battery. Furthermore, the EMS also achieves SOC_{UC} regulation thus guaranteeing the operation of the system. For future work, a low power prototype will be created, and the performance of the proposed EMS will be compared experimentally with an EMS based on FL

Table 1. Averages of absolute values of rate of power changes

	Initial SOC_{UC}=0.4	Initial SOC_{UC}=0.6
$\overline{\lvert\Delta P_{out}/\Delta t\rvert}$	14.66kW/s	
$\overline{\lvert\Delta P_{FC}/\Delta t\rvert}$	2 kW/s	2.01 kW/s
$\overline{\lvert\Delta P_{bat}/\Delta t\rvert}$	2.78 kW/s	2.75 kW/s
$\overline{\lvert\Delta P_{UC}/\Delta t\rvert}$	11.43 kW/s	11.84 kW/s

6. Acknowledgment

This work is supported by Düzce University Research Fund Project Number 2017.07.03.616.

7. References

[1] Kelouwani, S., Agbossou, K., Dubé, Y., and Boulon, L., "Fuel cell plug-in hybrid electric vehicle anticipatory and real-time blended-mode energy management for battery life preservation", Journal of Power Sources, 221, 406-418, 2013.

[2] Salisbury, S., "Understanding fuel cell plug-in hybrid electric vehicle use, design, and functionality" Diss. Colorado State University. Libraries, 2014.

[3] Marchesoni, M., and Camillo, V., "New DC–DC converter for energy storage system interfacing in fuel cell hybrid electric vehicles" , IEEE Transactions on Power Electronics, 22, 1,301-308, 2007.

[4] Shuai, L., Corzine, K. A., and Ferdowsi, M.. "A unique ultracapacitor direct integration scheme in multilevel motor drives for large vehicle propulsion", IEEE Transactions on Vehicular Technology 56,4, 1506-1515, 2007.

[5] Camara, M. B., Gualous, H., Gustin, F., Berthon, A., and Dakyo, B., "DC/DC converter design for supercapacitor and battery power management in hybrid vehicle applications—Polynomial control strategy", IEEE Transactions on Industrial Electronics 57, 2, 587-597, 2010.

[6] Samosir, A. S., and Yatim, A. H. M., "Implementation of dynamic evolution control of bidirectional DC–DC converter for interfacing ultracapacitor energy storage to fuel-cell system", IEEE Transactions on Industrial Electronics, 57, 10, 3468-3473, 2010.

[7] Payman, A., Pierfederici, S., Meibody-Tabar, F., and Davat, B., "An adapted control strategy to minimize DC-bus capacitors of a parallel fuel cell/ultracapacitor hybrid system", IEEE Transactions on Power Electronics, 26,12, 3843-3852, 2011.

[8] Nejabatkhah, F., Danyali, S., Hosseini, S. H., Sabahi, M., and Niapour, S. M., "Modeling and control of a new three-input DC–DC boost converter for hybrid PV/FC/battery power system", IEEE Transactions on Power Electronics, 27, 5, 2309-2324, 2012.

[9] Wai, R. J., Lin, C. Y., Liaw, J. J., and Chang, Y. R., "Newly designed ZVS multi-input converter", IEEE Transactions on Industrial Electronics, 58, 2, 555-566, 2011.

[10] Bauman, J., and Kazerani, M, "A comparative study of fuel-cell–battery, fuel-cell–ultracapacitor, and fuel-cell–battery–ultracapacitor vehicles", IEEE Transactions on Vehicular Technology, 57, 2, 760-769, 2008.

[11] Hu, X., Johannesson, L., Murgovski, N., and Egardt, B., "Longevity-conscious dimensioning and power management of the hybrid energy storage system in a fuel cell hybrid electric bus", Applied Energy, 137, 913-924, 2015.

[12] García, P., Torreglosa, J. P., Fernández, L. M., and Jurado, F., "Control strategies for high-power electric vehicles powered by hydrogen fuel cell, battery and supercapacitor", Expert Systems with Applications, 40, 12, 4791-4804, 2013.

[13] Di Napoli, A., Crescimbini, F., Rodo, S., and Solero, L., "Multiple input DC-DC power converter for fuel-cell powered hybrid vehicles", IEEE 33rd Annual Power Electronics Specialists Conference, 1685-1690, 2002.

[14] Solero, L., Lidozzi, A., and Pomilio, J. A, "Design of multiple-input power converter for hybrid vehicles", IEEE Transactions on Power Electronics, 20, 5, 1007-1016, 2005.

[15] Nejabatkhah, F., Danyali, S., Hosseini, S. H., Sabahi, M., and Niapour, S. M., "Modeling and control of a new three-input DC–DC boost converter for hybrid PV/FC/battery power system", IEEE Transactions on Power Electronics, 27, 5, 2309-2324, 2012.

[16] Akar, F., Tavlasoglu, Y., and Vural, B., "Analysis and experimental verification of a multi-input converter for DC microgrid applications", IET Power Electronics, 11,6, 1009-1017, 2014.

[17] Akar, F.. "A Bidirectional 3-Input DC-DC Converter for Electrical Vehicles", İleri Teknoloji Bilimleri Dergisi, 5, 2, 2016.

[18] Erdinc, O., and Uzunoglu, M., "Recent trends in PEM fuel cell-powered hybrid systems: Investigation of application areas, design architectures and energy management approaches.", Renewable and Sustainable Energy Reviews, 14, 9, 2874-2884, 2010.

[19] Melero-Pérez, A., Gao, W., and Fernández-Lozano, J. J., "Fuzzy logic energy management strategy for fuel cell/ultracapacitor/battery hybrid vehicle with multiple-input DC/DC converter", Vehicle Power and Propulsion Conference, 2009.

[20] Ibrahim, M., Jemei, S., Wimmer, G., and Hissel, D., "Nonlinear autoregressive neural network in an energy management strategy for battery/ultra-capacitor hybrid electrical vehicles", Electric Power Systems Research, 136, 262-269, 2016.

[21] Chen, Z., Xiong, R., and Cao, J., "Particle swarm optimization-based optimal power management of plug-in hybrid electric vehicles considering uncertain driving conditions", Energy, 96, 197-208, 2016.

[22] Chen, Z., Mi, C. C., Xiong, R., Xu, J., and You, C., "Energy management of a power-split plug-in hybrid electric vehicle based on genetic algorithm and quadratic programming", Journal of Power Sources, 248, 416-426, 2014.

[23] Liu, G., Zhang, J., and Sun, Y., "High frequency decoupling strategy for the PEM fuel cell hybrid system", International Journal of hydrogen energy, 33,21, 6253-6261, 2008.

[24] Zhang, X., Mi, C. C., Masrur, A., and Daniszewski, D., "Wavelet-transform-based power management of hybrid vehicles with multiple on-board energy sources including fuel cell, battery and ultracapacitor", Journal of Power Sources, 185, 2, 1533-1543, 2007.

[25] Lin, W. S., and Zheng, C. H. , "Energy management of a fuel cell/ultracapacitor hybrid power system using an adaptive optimal-control method", Journal of Power Sources, 196, 6, 3280-3289, 2011.

[26] Zandi, M., Payman, A., Martin, J. P., Pierfederici, S., Davat, B., and Meibody-Tabar, F., "Energy management of a fuel cell/supercapacitor/battery power source for electric vehicular applications", IEEE Transactions on Vehicular Technology, 60,2, 433-443, 2011.

[27] Motapon, S. N., Dessaint, L. A., and Al-Haddad, K., "A comparative study of energy management schemes for a fuel-cell hybrid emergency power system of more-electric aircraft", IEEE Transactions on Industrial Electronics, 61,3, 1320-1334, 2014.

[28] Hredzak, B., Agelidis, V. G., Demetriades, G. D. "A low complexity control system for a hybrid dc power source based on ultracapacitor–lead–acid battery configuration". IEEE transactions on Power Electronics, 29,6, 2882-2891, 2014.

[29] Curti, J. M. A., Huang, X., Minaki, R., and Hori, Y., "A simplified power management strategy for a supercapacitor/battery Hybrid Energy Storage System using the Half-Controlled Converter",. IECON 38th Annual Conference on IEEE Industrial Electronics Society, 4006-4011, 2012.

[30] Alloui, H., Achour, Y., Marouani, K., and Becherif, M., "Energy management based on frequency decoupling: experimental results with fuel cell-electric vehicle emulator", IEEE 81st Vehicular Technology Conference, 1-5, 2015.

[31] Alloui, H., Becherif, M., and Marouani, K. "Modelling and frequency separation energy management of fuel cell-battery hybrid sources system for hybrid electric vehicle", 21st IEEE Mediterranean Conference on Control and Automation ,646-651,2013.

[32] Blanes, J. M., Gutiérrez, R., Garrigós, A., Lizán, J. L., and Cuadrado, J. M., "Electric vehicle battery life extension using ultracapacitors and an FPGA controlled interleaved buck–boost converter", IEEE Transactions on Power Electronics, 28,12, 5940-5948, 2013.

[33] Uzunoglu, M., and Alam, M. S., "Modeling and analysis of an FC/UC hybrid vehicular power system using a novel-wavelet-based load sharing algorithm", IEEE Transactions on Energy Conversion, 23,1, 263-272, 2008.

[34] Campanari, S., Manzolini, G., and De la Iglesia, F. G., "Energy analysis of electric vehicles using batteries or fuel cells through well-to-wheel driving cycle simulations", Journal of Power Sources, 186, 2, 464-477,2009

.

Appendix A

$$v_{L1}=\begin{cases} v_{FC}-i_{L1}(R_{DS-ON}+R_L)-\left(\sum i_L\right)R_{DS-ON}, & 0\sim d_1T_S \\ -v_F-i_{L1}R_L-\left(\sum i_L\right)R_{DS-ON}, & d_1T_S\sim d_4T_S \\ -v_F-i_{L1}R_L-v_{SD}-v_o, & d_4T_S\sim T_S \end{cases} \quad (A.1)$$

$$v_{L2}=\begin{cases} v_{bat}-i_{L2}(R_{DS-ON}+R_L)-\left(\sum i_L\right)R_{DS-ON}, & 0\sim d_4T_S \\ v_{bat}-i_{L2}(R_{DS-ON}+R_L)-v_{SD}-v_o, & d_4T_S\sim d_2T_S \\ -v_F-i_{L2}R_L-v_{SD}-v_o, & d_2T_S\sim T_S \end{cases} \quad (A.2)$$

$$v_{L3}=\begin{cases} v_{UC}-i_{L3}(R_{DS-ON}+R_L)-\left(\sum i_L\right)R_{DS-ON}, & 0\sim d_4T_S \\ v_{bat}-i_{L3}(R_{DS-ON}+R_L)-v_{SD}-v_o, & d_4T_S\sim d_3T_S \\ -v_F-i_{L3}R_L-v_{SD}-v_o, & d_3T_S\sim T_S \end{cases} \quad (A.3)$$

$$v_{L3}=\begin{cases} v_{UC}+v_{SD}-i_{L3}R_L-\left(\sum i_L\right)R_{DS-ON}, & 0\sim d_4T_S \\ v_{UC}-i_{L3}R_L-v_o, & d_4T_S\sim T_S \end{cases} \quad (A.4)$$

$$v_{L1}=\begin{cases} v_{FC}-i_{L1}(R_{DS-ON}+R_L)-\left(\sum i_L\right)R_{DS-ON}-v_o, & 0\sim d_1T_S \\ -v_F-i_{L1}R_L-\left(\sum i_L\right)R_{DS-ON}-v_o, & d_1T_S\sim d_5T_S \\ -v_F-i_{L1}R_L+v_{SD}, & d_5T_S\sim T_S \end{cases} \quad (A.5)$$

$$v_{L2}=\begin{cases} v_{bat}-i_{L2}(R_{DS-ON}+R_L)-\left(\sum i_L\right)R_{DS-ON}-v_o, & 0\sim d_5T_S \\ v_{bat}-i_{L2}(R_{DS-ON}+R_L), & d_5T_S\sim d_2T_S \\ -v_F-i_{L2}R_L+v_{SD}, & d_2T_S\sim T_S \end{cases} \quad (A.6)$$

$$v_{L3}=\begin{cases} v_{UC}+v_{SD}-i_{L3}R_L-\left(\sum i_L\right)R_{DS-ON}-v_o, & 0\sim d_5T_S \\ v_{UC}+2v_{SD}-i_{L3}R_L, & d_5T_S\sim T_S \end{cases} \quad (A.7)$$